

ATMOSPHERIC SCIENCE

Atmospheric CO₂ levels from 2.7 billion years ago inferred from micrometeorite oxidation

O. R. Lehmer^{1,2,3*}, D. C. Catling^{1,2}, R. Buick^{1,2}, D. E. Brownlee^{2,4}, S. Newport¹

Earth's atmospheric composition during the Archean eon of 4 to 2.5 billion years ago has few constraints. However, the geochemistry of recently discovered iron-rich micrometeorites from 2.7 billion-year-old limestones could serve as a proxy for ancient gas concentrations. When micrometeorites entered the atmosphere, they melted and preserved a record of atmospheric interaction. We model the motion, evaporation, and kinetic oxidation by CO₂ of micrometeorites entering a CO₂-rich atmosphere. We consider a CO₂-rich rather than an O₂-rich atmosphere, as considered previously, because this better represents likely atmospheric conditions in the anoxic Archean. Our model reproduces the observed oxidation state of micrometeorites at 2.7 Ga for an estimated atmospheric CO₂ concentration of >70% by volume. Even if the early atmosphere was thinner than today, the elevated CO₂ level indicated by our model result would help resolve how the Late Archean Earth remained warm when the young Sun was ~20% fainter.

INTRODUCTION

The atmospheric CO₂ concentration of the Archean Earth is highly uncertain. In the Archean, the Sun was 20 to 30% less luminous and CO₂ levels would have needed to be much higher than modern to maintain a climate suitable for liquid water, perhaps by a factor of 10² to 10³, depending on the concentration of other greenhouse gases, such as CH₄ [e.g., (1, 2)]. In addition to atmospheric models, Archean paleosols and other proxies have been examined to constrain atmospheric CO₂ levels. Estimates from these studies range between ~3 × 10⁻³ and ~0.75 bar of CO₂ during the Archean [see section 11.4.3 of (3) for a review]. Thus, the estimated atmospheric CO₂ level in the Archean spans ~3 orders of magnitude.

The spread in the Archean atmospheric CO₂ concentrations is part of a debate about the climate of early Earth. Isotopic analyses of phosphates (4) and deuterium (5) suggest that the Archean surface temperature was temperate and <40°C. In addition, the presence of Archean glacial deposits [e.g., (6)] indicates early Earth was at least periodically cool. However, a high-temperature Archean with surface temperatures of 70 ± 15°C has been proposed on the basis of measurements of oxygen isotopes in Archean cherts (7). The possible presence of a low-viscosity Archean ocean (8) and the thermostability of resurrected Archean proteins (9) are also used for claiming a high-temperature Archean. Additional CO₂ estimates for the Archean atmosphere could help resolve this temperature uncertainty and provide insight into the conditions for life on early Earth.

It was recently proposed that Archean, spherical, iron-rich (type I) micrometeorites could have been oxidized by modern levels of O₂ in the upper atmosphere (10, 11). However, very low levels of O₂ in the Archean atmosphere inferred from a large variety of proxies [e.g., (12)] motivate considering oxidation by CO₂ as an alternative (13). Thus, the micrometeorites could provide a new constraint on Archean CO₂ levels.

When FeNi metal micrometeoroids enter the atmosphere at hypervelocity, they can melt, and while molten, they react readily with the surrounding atmosphere (14). During this reaction, iron micrometeorites exposed to O₂ or CO₂ can oxidize some or all of the metal to species such as wüstite [Fe_(1-x)O] and magnetite (Fe₃O₄) (15). Depending on size, entry speed, and entry angle, the micrometeorites melt and oxidize in the upper atmosphere for only a few seconds at approximately 75 to 90 km above the surface for modern Earth and solidify well before reaching the lower atmosphere. After solidifying in the upper atmosphere, iron-rich micrometeorites become largely inert and can preserve their oxidation state through geologic time (10).

The possibility that Archean micrometeorites could provide a proxy for atmospheric composition was first proposed by Tomkins *et al.* (10). They found 59 iron-rich micrometeorites in a 2.7 billion-year-old limestone from the Pilbara region of northwestern Australia that contained magnetite, wüstite, and metallic iron. Tomkins *et al.* concluded that micrometeorite oxidation most likely occurred in Earth's atmosphere and suggested that ~20% atmospheric oxygen in the upper atmosphere was responsible. They discounted CO₂ in favor of oxidation from atmospheric O₂ because of slow kinetics in low-temperature (1100 K), high-pressure (1 bar) laboratory measurements of oxidation of solid (and not molten) Fe by CO₂ and their equilibrium-based calculations, which implied that small, iron-rich micrometeorites would not be oxidized in a low-CO₂ atmosphere (<10% by volume). They also note that a CO₂-rich atmosphere could contain some CO, a reductant. However, such an atmosphere should also produce O₂ and O₃ [e.g., (16)], which could mitigate the reducing capacity of CO. In addition, Fe-rich micrometeorites melt for only a few seconds during entry and likely do not reach equilibrium during this time (10), making it premature to rule out CO₂ as a plausible oxidant.

While an oxygen-rich atmosphere is certainly capable of oxidizing iron micrometeorites, an upper atmosphere of ~20% O₂ is difficult to reconcile with evidence for an anoxic atmosphere in the Archean where O₂ was likely less than 10⁻⁴ bar at altitude (17) and less than 1 ppmv (parts per million by volume) at ground level (12, 18–20). In addition to proxy data showing low atmospheric O₂ in the Archean, current understanding of atmospheric mixing does not support an

Copyright © 2020
The Authors, some
rights reserved;
exclusive licensee
American Association
for the Advancement
of Science. No claim to
original U.S. Government
Works. Distributed
under a Creative
Commons Attribution
License 4.0 (CC BY).

¹Department of Earth and Space Sciences, University of Washington, Seattle, WA 98195, USA. ²Astrobiology Program, University of Washington, Seattle, WA 98195, USA. ³MS 239-4, Space Science Division, NASA Ames Research Center, Moffett Field, CA 94035, USA. ⁴Department of Astronomy, University of Washington, Seattle, WA 98195, USA.

*Corresponding author. Email: info@lehmer.us

O₂-rich Archean upper atmosphere with anoxic lower atmosphere. Turbulent mixing, particularly from breaking gravity waves (which physics dictates increase in amplitude with altitude), mixes the major constituents of the atmosphere up to the homopause at ~100-km altitude on modern Earth. Such waves are shed from airflow over surface topography, jets, and thermal tides, which are all processes that would have occurred on ancient Earth.

The homopause is the pressure, or altitude, below which the major atmospheric constituents are well mixed due to turbulence, and on modern Earth is well above the melting altitude for micrometeorites between roughly 65 and 90 km. It is tempting to speculate that the homopause may have occurred at a higher pressure on Archean Earth, and thus at a lower altitude, more consistent with the melting of micrometeorites. However, a high-pressure homopause in the Archean would be physically unusual compared with all other known terrestrial atmospheres. In the Solar System, rocky bodies have homopause pressures of $\sim 10^{-2}$ Pa on Earth, $\sim 10^{-2}$ to $\sim 10^{-5}$ Pa on Mars (depending on season) (21), $\sim 10^{-3}$ Pa on Venus, and $\sim 10^{-4}$ Pa on Titan [(3), p. 6]. Thus, a high-pressure homopause on Archean Earth may be counter to current understanding of atmospheric mixing and available data [see sections 4.3 and 4.4 of (3) for a detailed discussion of atmospheric mixing]. Even if the ground-level atmospheric pressure in the Archean were lower than modern (22, 23), the upper atmosphere would still be in approximate hydrostatic equilibrium. So, a lower ground-level pressure would not alter the absolute pressure aloft at which micrometeorites melt (10). An Archean model with constant vertical eddy mixing coefficient of 10^5 cm² s⁻¹ (11) produces high O₂ at altitude, but the assumed eddy mixing is an order to orders of magnitude lower than that determined empirically for the upper atmosphere of modern Earth ($\sim 10^6$ cm² s⁻¹) (24) or required to model the thin atmosphere of Mars (e.g., 10^6 cm² s⁻¹ at 20-km to 4×10^7 cm² s⁻¹ at 80-km altitude) (25).

For all the above reasons, we propose a CO₂-rich atmosphere capable of oxidizing Fe micrometeorites may have been present at 2.7 Ga. A CO₂-rich atmosphere is consistent with geochemical analyses of the acid weathering of Archean soils that became paleosols [e.g., (26)] and agrees with current models of the Archean carbon cycle and climate (2), and demands no peculiar set of circumstances to create high upper atmosphere O₂ in an anoxic Archean. Furthermore, it has long been demonstrated in the metallurgy industry that CO₂ can oxidize metallic Fe under various atmospheric conditions and temperatures [e.g., (27)].

By modeling the motion, heating, and evaporation of micrometeorites during atmospheric entry, and using a rate constant for Fe oxidation via CO₂ from laboratory measurements (28) (see Materials and Methods for details), we investigate what atmospheric CO₂ levels could explain the reported oxidation of Archean micrometeorites. In this way, we seek to provide a new constraint on atmospheric CO₂ levels during the Archean.

RESULTS

We model 15,000 randomly generated micrometeorites entering a 1 bar N₂-CO₂ atmosphere with CO₂ concentrations between ~2 and ~85% by volume [3 to 90 weight % (wt %)]. We assume that all particles start as pure Fe upon entry. Our model tracks the motion, oxidation, and evaporation of each particle, along with its composition throughout its descent in the atmosphere. We look at the cross

section of each simulated micrometeorite and compare the total area of unoxidized Fe to the total cross-sectional area of the particle (i.e., oxidized Fe area plus unoxidized Fe area). We chose to measure the cross-sectional area to make empirical micrometeorite data readily comparable to our model results. Figure 1 shows an example of our model for a single micrometeorite entering a 39% CO₂, 61% N₂ atmosphere.

The atmosphere of the Archean was O₂ poor [e.g., (29)]. However, photochemical models of Earth-like planets around Sun-like stars

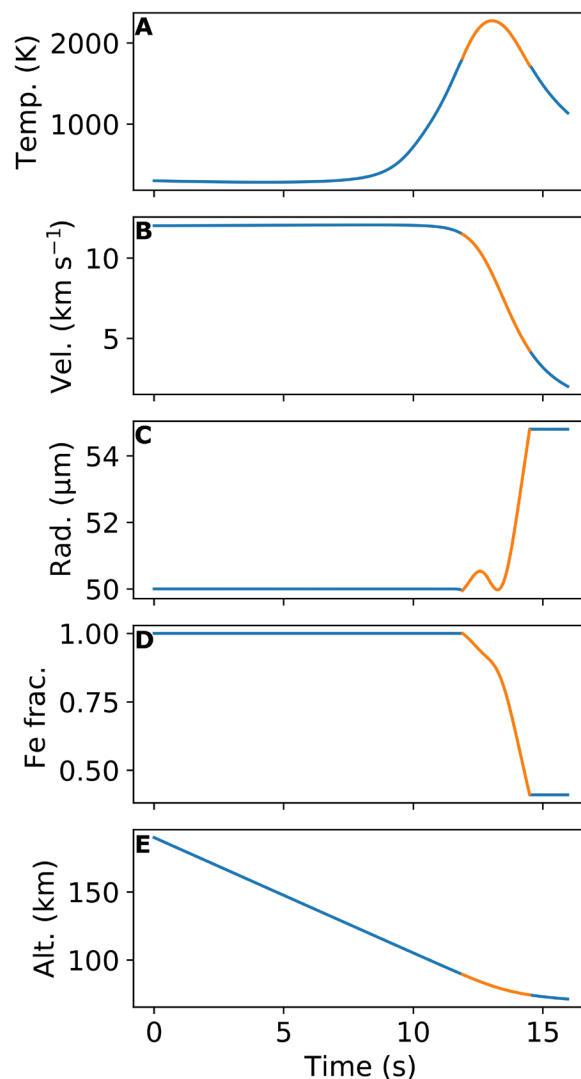


Fig. 1. Single model run for a particle with an entry angle of 45° from zenith through a 39% CO₂, 61% N₂ atmosphere (50 wt % CO₂, 50 wt % N₂). The plots above show (A) micrometeorite temperature in kelvin, (B) micrometeorite velocity in kilometers per second, (C) micrometeorite radius in micrometers, (D) mass fraction of metallic Fe to oxidized FeO, and (E) micrometeorite's altitude above Earth's surface in kilometers. The orange part of each curve indicates the micrometeorite is molten. For plot (C), the micrometeorite increases in radius because the oxide layer is growing faster than it is evaporating. The oxidation of high-density Fe to the lower-density FeO results in a less dense particle and, thus, a larger radius. In this simulation, the micrometeorite is molten for 2.6 s between 11.9 and 14.5 s. The initial radius is 50 μm, the final radius is 54.8 μm, the final Fe fractional mass is 41% (37% by cross-sectional area), and the maximum temperature reached is 2275 K at an altitude of 81.2 km. See the Supplementary Materials for an animation of this figure.

indicate that minor atmospheric O_2 could be sustained photochemically in the upper atmosphere via CO_2 photolysis. From such models, the O_2 level in the upper atmosphere could reach $\sim 1\%$ by volume in a high (90% by volume) CO_2 atmosphere while remaining a trace gas at the planetary surface (16). This O_2 concentration is well below the modern levels required to explain the oxidation of Archean micrometeorites (10).

To address the possibility of oxidation by major CO_2 and minor O_2 in the Archean, we ran our model with a CO_2 - N_2 - O_2 atmosphere. Each of the 15,000 modeled micrometeorites was simulated, entering both a CO_2 - N_2 -only atmosphere and a CO_2 - N_2 - O_2 (1%) atmosphere. As an upper bound, the atmospheric O_2 was fixed at 1% and did not decrease with altitude in the altitude range for micrometeorite melting. The results of both runs are shown in Fig. 2. The black curve in Fig. 2 shows the mean unoxidized Fe fractional area in our modeled micrometeorites as atmospheric CO_2 increases for the CO_2 - N_2 atmosphere, while the orange curve shows the same for micrometeorites entering the CO_2 - N_2 - O_2 (1%) atmosphere. The difference in final Fe fractional area between the two atmospheres is negligible, especially at high CO_2 concentrations, showing that CO_2 dominates as the oxidant when O_2 is $\sim 1\%$ or lower.

The Archean CO_2 estimates from the modeling are shown in Fig. 3 (the black line of Fig. 3 is the same as in Fig. 2). On average, we find that the unoxidized Fe fractional area of sectioned micrometeorites decreases monotonically as atmospheric CO_2 concentrations increase. The solid black curve in Fig. 3 shows the mean unoxidized Fe area in our modeled micrometeorites as atmospheric CO_2 increases. The gray-shaded region is the model 2σ uncertainty arising from uncertainties in initial mass, velocity, and impact angle (see Materials and Methods). The orange dot and error bar show the mean fractional Fe area measured by Tomkins *et al.*

From the black curve in Fig. 3, we estimate an Archean CO_2 volume mixing ratio of $64_{-58}^{+36}\%$ (2σ) given the data from Tomkins *et al.* (orange dot and error bar in Fig. 3). The uncertainty is large because of the paucity of Archean micrometeorite data: Only two data points are available with metallic Fe fractional areas of 0.555 and 0.003, respectively (inferred from Tomkins *et al.*'s Fig. 1, E and F).

Some fully oxidized micrometeorites collected by Tomkins *et al.* indicate that high CO_2 levels were likely present during entry. Our model predicts that fully oxidized micrometeorites will only form when atmospheric CO_2 concentrations exceed $\sim 70\%$ by volume, as indicated by the dashed blue curve in Fig. 4. As such, while our CO_2

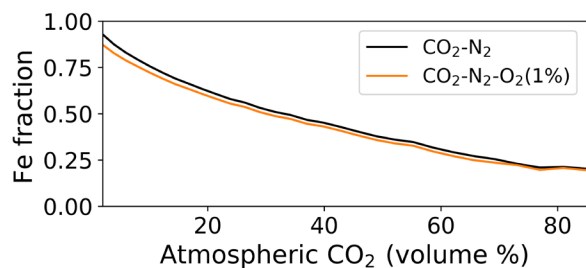


Fig. 2. Comparison of unoxidized Fe area in CO_2 - N_2 and CO_2 - N_2 - O_2 atmospheres with increasing CO_2 . The black curve shows the mean model cross-sectional area of unoxidized Fe compared with the total cross-sectional area of the micrometeorite for a CO_2 - N_2 atmosphere. It is the same curve as in Fig. 3. The orange contour shows the same simulated micrometeorites but entering a CO_2 - N_2 - O_2 atmosphere where the O_2 represents 1% by volume. The addition of 1% O_2 to the atmosphere has little impact on the average.

estimate spans 6% to 100% (2σ), the CO_2 concentration likely falls above $\sim 70\%$ given the presence of some fully oxidized micrometeorites in the Tomkins *et al.* data. This agrees with Archean paleosols and climate models of Archean Earth, which suggest that CO_2 levels on the Archean were substantially higher than modern. If Archean Earth had a 1-bar atmosphere, then our estimate of $>70\%$ CO_2 by volume indicates that the partial pressure of CO_2 would be >0.7 bar in the Archean. However, surface pressure may have been much lower during the Archean, perhaps just 0.23 ± 0.23 bar (2σ) (22). With a mean surface pressure of 0.23 ± 0.23 bar, our model predicts a CO_2 partial pressure of $>0.16 \pm 0.16$ bar (2σ). Provided some methane was present, such as 0.5% (30), this thin, CO_2 -rich atmosphere could provide enough greenhouse warming to sustain liquid water under a faint young Sun [e.g., (31)]. Atmospheric methane would warm the surface during the Archean as a greenhouse gas but is not expected to interact with molten, Fe-rich micrometeorites (10) and thus should not alter their oxidation state.

In our model, the oxidation of micrometeorites in the upper atmosphere is not affected by the atmospheric surface pressure. Reducing the surface pressure would move the altitude at which micrometeorites oxidize closer to the surface (slightly altering the gravitational acceleration experienced by melting micrometeorites), but the overall pressures at which melting occurs do not appreciably change nor do our results. The difference in model results between a 1-bar atmosphere and a 0.23-bar atmosphere is negligible, which agrees with the findings of Tomkins *et al.*

DISCUSSION

Our model shows that 2.7 billion-year-old micrometeorites (10) could have been oxidized by CO_2 in a CO_2 -rich atmosphere. While our estimated CO_2 abundance of $64_{-58}^{+36}\%$ (2σ) has large uncertainties, collection and analysis of additional Archean micrometeorites could greatly reduce the spread in this estimate. Using the parameterized climate model described in (2), $\sim 70\%$ CO_2 for the Archean atmosphere, and an upper bound on Archean surface pressure of ~ 0.5 bar (22), the global mean surface temperature in the Archean would be $\sim 30^\circ C$ (or lower for lower total pressure), indicating a temperate Archean climate. An improved Archean CO_2 measurement would allow more robust climate models to further refine the surface temperature of Archean Earth and the conditions, including pH of surface waters, in which early life evolved. Not only would this help address the hot versus temperate Archean debate, but it could also inform our understanding of Earth-like exoplanets and their potential habitability [e.g., (32)].

The uncertainty in our model output (gray-shaded region in Fig. 3) is more difficult to reduce. This uncertainty stems from the random sampling of our initial parameter distributions for mass, velocity, and entry angle, which have some inherent uncertainty on modern Earth (see Materials and Methods). Despite such uncertainties, our model can reasonably predict the Fe fractional area in modern micrometeorites entering an O_2 -rich atmosphere (e.g., Fig. 4).

The conclusion that a CO_2 -rich atmosphere can oxidize Fe micrometeorites is a reasonable alternative to oxidation via the O_2 -rich Archean atmospheres (10, 11). As demonstrated by the metallurgy industry [e.g., (27)] and other laboratory measurements (28), CO_2 can readily oxidize Fe, albeit less efficiently than O_2 . While we do not model oxidation past FeO, further oxidation is not precluded by our model as the oxide that forms during entry is a liquid Fe melt

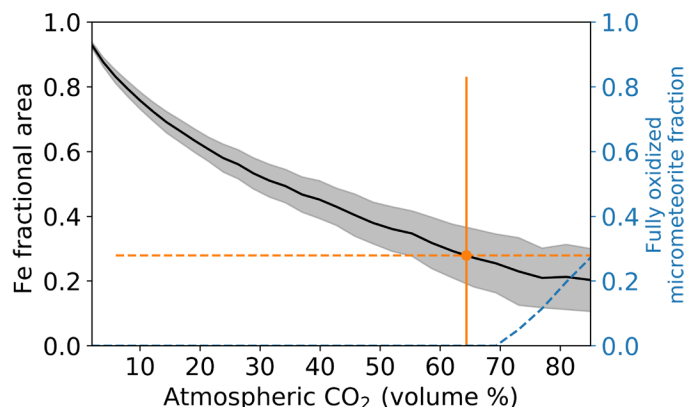


Fig. 3. Simulated fractional area of unoxidized Fe with increasing atmospheric CO₂. The atmosphere was assumed to be composed of pure N₂ and CO₂. The black curve shows the mean model prediction for the cross-sectional area of unoxidized Fe compared with the total cross-sectional area of the micrometeorite. The simulated micrometeorites were assumed to have spherical, central metal beads so the cross-sectional area of the unoxidized Fe bead is a maximum. The gray-shaded area shows the 2σ confidence interval of our model. The orange dot and solid error bar show the mean unoxidized Fe fractional area and 2σ confidence interval from the two Fe-FeO micrometeorites reported by Tomkins *et al.* (10). The corresponding uncertainty in atmospheric CO₂ from the Tomkins *et al.* data is shown by the dashed orange error bars. The Tomkins *et al.* data point indicates the CO₂ level was at 64⁺³⁶₋₅₈% (2σ). The dashed blue line shows the fraction of modeled micrometeorites that were fully oxidized in the atmosphere with no remaining metallic Fe. Such particles could lead to magnetite-rich micrometeorites and appear in our model once atmospheric CO₂ reaches ~70%.

with dissolved oxygen [see (14) for a discussion]. If the melt acquires more O than Fe, then it could solidify as Fe₃O₄ rather than FeO. However, additional laboratory measurements of molten Fe beads quenching in simulated CO₂-rich atmospheres are necessary to understand how CO₂ oxidizes Fe liquids at high temperatures.

Our model results in Fig. 3 show that a >70% by volume CO₂ atmosphere could fully oxidize micrometeorites and possibly produce magnetite. This is seen by the dashed blue line in Fig. 3, which shows the fraction of the total simulated micrometeorites that are fully oxidized after entry as a function of atmospheric CO₂ abundance. Our simulation stops when a micrometeorite has no remaining unoxidized Fe, but such a micrometeorite encountering additional CO₂ could continue to oxidize past FeO, possibly to Fe₃O₄ (see Materials and Methods).

In addition to showing that atmospheric CO₂ could explain the observed, oxidized Archean micrometeorites, our model predicts that the average unoxidized Fe remaining in collected micrometeorites should decrease with increasing atmospheric CO₂. From this relationship, it may be possible to constrain atmospheric CO₂ concentrations not only in the Archean but also in the Proterozoic when atmospheric oxygen was scarce. Our CO₂-N₂-O₂ atmosphere with 1% O₂ in the upper atmosphere could be representative of the Proterozoic atmosphere (29) in which micrometeorite oxidation would still be dominated by CO₂, as seen in Fig. 2 (orange curve). Numerous iron-rich micrometeorites have been found in Proterozoic rocks (33) and measuring the fractional area of unoxidized Fe in such samples could readily be done. Such measurements might provide a constraint on atmospheric CO₂ at that time.

The CO₂ concentration of the atmosphere is thought to have decreased over Earth's history [e.g., (2)] from a major atmospheric

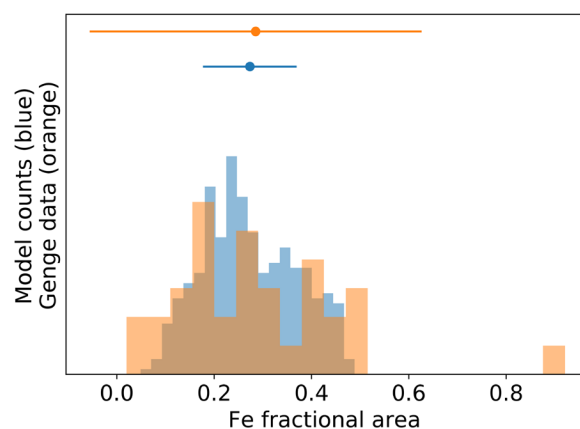


Fig. 4. Fractional area of unoxidized Fe in simulated sectioned micrometeorites compared with observed modern micrometeorites. The horizontal axis in this plot shows the fractional area of unoxidized Fe in cross-sectioned micrometeorites. The blue histogram shows the simulated unoxidized Fe fractional area from 500 randomly generated micrometeorites entering the modern atmosphere, which were oxidized by O₂, and the orange histogram shows the data inferred from figure 4 of Genge *et al.* (15). The model mean and 2σ confidence interval are shown by the blue dot and error bar, while the mean and 2σ of the data from Genge *et al.* are shown by the orange dot and error bar.

constituent in the Archean to a few hundred parts per million today. If we compare that trend to the black curve in Fig. 3, we see that our model predicts the fractional area of unoxidized Fe in collected micrometeorites should increase with time—if the trend depends just on CO₂ oxidation—from the Archean until the end of the Neoproterozoic, albeit with some uncertainty due to a possible O₂ overshoot during the Great Oxidation Event. Oxidation by O₂ might remain minor during the Proterozoic because the ground-level atmospheric O₂ may have been ~0.2% absolute concentration or less (29) so the trend could hold (Fig. 2, orange curve). To verify this hypothesis, additional micrometeorites should be collected and analyzed.

MATERIALS AND METHODS

Experimental design

Model description

This work follows the models developed by Love and Brownlee (34) (hereafter LB) and Genge (14) (hereafter MG). The LB model describes the entry and evaporation of silicate micrometeorites on modern Earth. The MG model expands the model of LB to include Fe-rich micrometeorites and their oxidation during atmospheric entry. Below, we describe our model, which is an implementation of the MG model but for oxidation of Fe by CO₂.

Following MG and LB, our model describes the motion, heating, evaporation, and oxidation of iron micrometeorites. We assume an initial velocity, v (m s⁻¹), an initial mass, m (kg), and an initial entry angle from zenith θ with $\theta = 90^\circ$ being tangential to Earth's surface and $\theta = 0^\circ$ indicating the particle is moving directly toward Earth's surface. The motion of the particle in two dimensions, accounting for atmospheric drag, can be calculated via

$$\frac{dv}{dt} = g - \frac{3\rho_a v^2}{4\rho r} \hat{v} \quad (1)$$

where g is gravity (m s⁻²), v is velocity (m s⁻¹), t is time (s), ρ_a is the atmospheric density (in kg m⁻³), ρ is the density of the micrometeorite

(kg m^{-3}), and r is the particle radius (m). The altitude, a , of the particle was assumed to start at 190 km above Earth's surface, following LB, and tracked throughout the model. For a given altitude, g is easily calculated from $g = GM_{\oplus}/r_{\text{alt}}^2$ for gravitational constant $G = 6.67 \times 10^{-11} \text{ N m}^2 \text{ kg}^{-2}$ and Earth mass $M_{\oplus} = 5.97 \times 10^{24} \text{ kg}$; here, r_{alt} is the radial distance from the center of Earth to altitude, a . The MSIS-E-90 Atmosphere Model (available at https://ccmc.gsfc.nasa.gov/modelweb/models/msis_vitmo.php) was used to generate an atmospheric density profile for modern Earth, which we used for both the modern and Archean atmospheres following (35). Even if the atmospheric pressure in the Archean were lower than modern (22), the density profile of the upper atmosphere generated by the MSIS-E-90 model would likely remain similar and produce similar model results, as noted by (10).

We used the MSIS-E-90 model to generate atmospheric densities, ρ_a , and total atmospheric oxygen densities (both O and O_2) at 1-km intervals from Earth's surface to 190 km (see data file S1 atmosphere_data.txt for MSIS-E-90 input parameters and resulting data). We linearly interpolated between each data point to find the atmospheric density for a given altitude. When calculating atmospheric CO_2 abundance in the model, we specify a CO_2 wt %, and then multiply the wt % by ρ_a . This was done to make conversions from the MSIS-E-90 density data to CO_2 abundances a simple conversion. For example, if the model is run with 30 wt % CO_2 , then the atmospheric CO_2 density will be found via $0.3\rho_a$, with ρ_a coming directly from the MSIS-E-90 data. When modeling CO_2 atmospheres, we assume the remainder of the atmosphere is N_2 .

With the velocity of the micrometeorite known, the heat flux of the particle, dq/dt , in watts can be described by

$$\frac{dq}{dt} = \frac{\pi r^2 \rho_a v^3}{2} - L_v \frac{dm_{\text{evap}}}{dt} - 4\pi r^2 \sigma T^4 + \Delta H_{\text{ox}} \frac{dm_{\text{ox}}}{dt} \quad (2)$$

following equations 3 and 14 from MG. The first term on the right hand side of Eq. 2 describes the heat flux due to collisions with air, which incorporates the ram pressure, $\rho_a v^2$, experienced by the micrometeorite. The second term describes the heat flux due to evaporative mass loss with the latent heat of vaporization for both FeO and Fe given by $L_v = 6 \times 10^6 \text{ J kg}^{-1}$ and the mass loss given by dm_{evap}/dt (in kg s^{-1}). The third term accounts for radiative heat loss with the Stefan-Boltzmann constant $\sigma = 5.67 \times 10^{-8} \text{ W m}^{-2} \text{ K}^{-4}$ and micrometeorite temperature T (in K). We assume a blackbody emissivity of unity for the radiative term, following MG. The final term describes the heat of oxidation of an Fe particle with dm_{ox}/dt being the mass growth of the oxide layer (in kg s^{-1}). From MG, Fe oxidation by oxygen is exothermic, with an oxidation enthalpy of $\Delta H_{\text{ox}} = 3.716 \times 10^6 \text{ J kg}^{-1}$. Oxidation by CO_2 is endothermic and has an oxidation enthalpy of $\Delta H_{\text{ox}} = -4.65 \times 10^5 \text{ J kg}^{-1}$.

Following MG, the ΔH_{ox} for CO_2 is approximated from the standard enthalpies of formation at standard temperature and pressure. It is estimated for the reactants and products in



where the energies for Fe, CO_2 , FeO, and CO are 0, -393.5 (36), -249.5 (37), and $-110.5 \text{ kJ mol}^{-1}$ (37), respectively. Putting these values into Eq. 3, we see that 33.5 kJ mol^{-1} is consumed in the reaction, or $4.65 \times 10^5 \text{ J kg}^{-1}$ of FeO. The heat of oxidation has only minor impact on the model results, so we neglect the temperature dependence of ΔH_{ox} following MG. The ΔH_{ox} for CO_2 is an order of

magnitude smaller than for O_2 in absolute value, so this assumption is especially reasonable for the CO_2 -rich atmosphere modeled here. It has been argued that the reaction described in Eq. 3 is the only plausible pathway of oxidation of Fe by CO_2 under the conditions considered in this work, so we do not consider other Fe + CO_2 products (28).

The heat flux can be related to the specific heat capacity, and to temperature via

$$\frac{dq}{dt} = mc_{\text{sp}} \frac{dT}{dt} \quad (4)$$

for mass m and specific heat of wüstite $c_{\text{sp}} = 400 \text{ (J kg}^{-1} \text{ K}^{-1})$, which coats the molten Fe micrometeorite upon entry (38). As shown in MG, Eqs. 2 and 4 give an equation for rate of temperature change

$$\frac{dT}{dt} = \frac{1}{rc_{\text{sp}}\rho} \left(\frac{3\rho_a v^3}{8} - \frac{3L_v}{4\pi r^2} \frac{dm_{\text{evap}}}{dt} - 3\sigma T^4 + \frac{3\Delta H_{\text{ox}}}{4\pi r^2} \frac{dm_{\text{ox}}}{dt} \right) \quad (5)$$

Equation 5 is the same as equation 6 of MG, but with the heat of oxidation term included. We note that MG is missing a 3 in the $3\sigma T^4$ term, likely due to a typesetting error.

In our model, we assume that Fe is only oxidized to FeO and do not consider further oxidation, following MG, as the process of oxidation past FeO is uncertain. As such, we only consider the ratio of unoxidized Fe to oxidized Fe in micrometeorites that are not fully oxidized in our model results. Following MG, we assume that any liquid oxide that forms during melting is immiscible with the molten Fe core and coats the exterior of the micrometeorite. Thus, we can calculate the evaporative mass loss rate, dm_{evap}/dt , by considering the rate of FeO (or Fe) evaporation using the Langmuir approximation, which is given by

$$\frac{dm_{\text{evap}}}{dt} = -4\pi r^2 p_v \sqrt{\frac{M}{2\pi R_{\text{gas}} T}} \quad (6)$$

where $R_{\text{gas}} = 8.314 \text{ J mol}^{-1} \text{ K}^{-1}$ is the ideal gas constant, M is the molar mass ($0.0718 \text{ kg mol}^{-1}$ for FeO or $0.0558 \text{ kg mol}^{-1}$ for Fe), and p_v is the vapor pressure of the evaporating FeO or Fe (in Pa). The vapor pressure was determined experimentally by Wang *et al.* (39) and from MG is given by

$$\log(p_v) = 10.3 - 20126/T \quad (7)$$

for FeO (note that Eq. 7 is the same as MG's equation 13 but for units of Pa rather than dynes cm^{-2}).

In addition to evaporation of the liquid oxide layer, our model allows the unoxidized Fe to evaporate as well. This is necessary because we consider low- CO_2 atmospheres where the formation of a liquid oxide layer surrounding the micrometeorite can be slower than the rate of evaporation. To handle this in our model, at each time step we calculate the oxide mass loss rate via Eq. 6, and if it exceeds the total oxide mass remaining in the particle, we evaporate liquid Fe for the remainder of the time step. The liquid Fe evaporation is calculated from Eq. 6 as well, but p_v is defined by

$$\log(p_v) = 11.51 - 1963/T \quad (8)$$

from the data in (39). Thus, the total evaporation can be given by

$$\frac{dm_{\text{evap}}}{dt} = \frac{dm_{\text{evap}_m}}{dt} + \frac{dm_{\text{evap}_\text{ox}}}{dt} \quad (9)$$

where dm_{evap_m}/dt is the metallic Fe evaporated and $dm_{\text{evap}_\text{ox}}/dt$ is the Fe oxide evaporated via Eq. 6.

The final step is to track the mass of Fe metal and FeO oxide in the micrometeorite. In an oxygen-rich atmosphere, we assume the total oxygen accumulated by the micrometeorite is given by

$$\frac{dO}{dt} = \gamma \rho_O \pi r^2 v \quad (10)$$

where ρ_O is the total density of oxygen (both O and O₂) encountered (in kg m⁻³), following MG. The γ term is a dimensionless factor between 0 and 1 that determines what fraction of the encountered oxidant is used to oxidize Fe ($\gamma = 1$ in this work, see MG for a discussion of γ and O₂).

For oxidation by CO₂, we calculate the reaction rate of Fe and CO₂ from

$$r_{CO_2} = k [Fe][CO_2] \quad (11)$$

for rate constant $k = 2.9 \times 10^8 \exp(-15155/T) \text{ m}^3 \text{ mol}^{-1} \text{ s}^{-1}$ from (28) with r_{CO_2} in mol m⁻³ s⁻¹. The Fe concentration is given by

$$[Fe] = \frac{m_{Fe}}{V} \quad (12)$$

where m_{Fe} is the mass of Fe in the micrometeorite (in mol), and V is the volume of the micrometeorite (in m³). The CO₂ concentration per unit volume is given by the total CO₂ encountered per second multiplied by the time step, Δt , i.e.

$$[CO_2] = \frac{\gamma \rho_{CO_2} \pi r^2 v}{V} \Delta t \quad (13)$$

where ρ_{CO_2} is in mol m⁻³. We compare the rate in Eq. 11 to the total CO₂ encountered per unit volume per time step and take the lesser of the two as the amount of oxygen accumulated by the Fe. We assume $\gamma = 1$ in Eq. 13, so the oxidation from CO₂ calculated with this model should be considered an upper bound. From Eq. 3, each CO₂ that reacts with the micrometeorite will add one O to the particle as FeO so

$$\frac{dO}{dt} = V \cdot \min\left(\frac{[CO_2]}{\Delta t}, r_{CO_2}\right) \quad (14)$$

When calculating dO/dt for CO₂, we first calculate in mol s⁻¹ and then convert to kg s⁻¹ for ease of use in the model.

It is important to note that the reaction rate for Fe oxidation via CO₂ used in this model was derived from laboratory measurements of gas-phase interactions of Fe and CO₂ (28). This likely represents an upper bound on Fe oxidation via CO₂ and may overestimate the oxidation of liquid Fe in a CO₂-rich atmosphere, where diffusion of the oxidant through the liquid Fe oxide could be the rate-limiting step. However, the kinetics of the reaction for the pressures and temperatures considered in this model are uncertain (noting that temperatures often exceed ~2000 K). As such, the model presented here should be considered an upper bound on the oxidation rate by CO₂. Future laboratory measurements are desirable to constrain the reaction rate described by Eq. 11.

Following MG, our model only allows oxidation, while unoxidized Fe remains in the micrometeorites. Thus, one Fe atom will be removed from the metallic Fe mass for each O atom accumulated. The total metallic Fe in the particle at each time step is then calculated by the amount Fe converted to Fe oxide, minus evaporated Fe, giving an equation for the mass of metallic Fe in the particle

$$\frac{dm_m}{dt} = \frac{M_{Fe}}{M_O} \frac{dO}{dt} - \frac{dm_{evap_m}}{dt} \quad (15)$$

for Fe molar mass $M_{Fe} = 0.0558 \text{ kg mol}^{-1}$ and atomic O molar mass $M_O = 0.0160 \text{ kg mol}^{-1}$. Similarly, the mass of oxide will grow for each O atom encountered, minus the evaporated FeO, which can be described by

$$\frac{dm_{ox}}{dt} = \frac{M_{FeO}}{M_O} \frac{dO}{dt} - \frac{dm_{evap_ox}}{dt} \quad (16)$$

With initial altitude, velocity, and mass known, Eqs. 1, 5, 9, 15, and 16 can be solved numerically to simulate the entry of an Fe micrometeorite. We assume all particles start as pure Fe and use a simple Euler approximation to numerically integrate the equations. We set the maximum time step to 0.01 s for our integration but allow the time step to adjust dynamically such that the maximum change in temperature of the particle never exceeds 0.1%. Following MG, we assume that no oxidation occurs until the micrometeorite melts at 1809 K for Fe and oxidation shuts off when the micrometeorite solidifies at 1720 K (the FeO melting temperature). We assume the liquid FeO has a density of 4400 kg m⁻³ and Fe has a density of 7000 kg m⁻³, from MG. In addition, for Fe, we use a specific heat of 400 J K⁻¹ kg⁻¹. The Python script containing our model is available in the Supplementary Materials. Figure 1 shows an example model run for a single 50- μm particle entering a 50 wt% CO₂, 50 wt% N₂ atmosphere at 12 km s⁻¹, and an entry angle of 45° from the Zenith.

Of interest in our model is the fractional area of unoxidized Fe compared with the total cross-sectional area of the micrometeorite (i.e., unoxidized Fe plus oxidized Fe) after they solidify. For a given micrometeorite, we assume that the unoxidized Fe forms a spherical bead at the center of the particle and is evenly surrounded by any produced oxide (FeO). We then “sectioned” the simulated micrometeorites at the midpoint and compared the total surface area of exposed metallic Fe to the total area of the sectioned micrometeorite. This quantity can be easily compared to measurements like those in figure 4 of (15), which reports Fe-phase abundance in sectioned micrometeorites. Our assumption that the metallic Fe is centered in the micrometeorite means we assume an upper bound on the sectioned area, as an uncentered bead may not measure Fe at the widest point. Despite this assumption, our model is able to accurately reproduce the data reported in figure 4 of (15), which shows the ratio of metallic Fe to oxidized Fe for 34 modern micrometeorites collected from Antarctica (we consider both FeO and Fe₃O₄ as oxides here and do not differentiate between them). Note that in (15), the captions of figures 4 and 5 are switched so the interested reader should look at the data presented in figure 4, but apply the caption of figure 5 to avoid confusion. Figure 4 in this paper shows our model prediction of Fe fractional area compared with the data inferred from figure 4 of (15). The agreement between our simulated data (blue) and the modern micrometeorite collected data (orange) is shown in the figure.

Following MG, we do not consider magnetite formation in our model because the process by which magnetite forms during entry is uncertain. The liquid Fe oxide that forms while the micrometeorite is molten could crystallize as Fe₃O₄ if enough oxygen is accumulated while molten. However, magnetite may also form after solidification due to decomposition of FeO to Fe₃O₄ or possibly from further oxidation at low temperatures. In addition, the central Fe bead could separate from the molten micrometeorite during entry, leading to a highly oxidized melt as a remainder, which could solidify as magnetite [see (14) for a discussion of Fe₃O₄ formation]. Thus, we only consider micrometeorites that still retain unoxidized Fe in both our model

results and collected data and do not differentiate between the phases of oxidized Fe.

When calculating our simulated micrometeorite areas, we impose several conditions on the final particle. First, we do not consider simulated particles that are smaller than 2 μm in final radius. Despite the abundance of such small particles, they are not easily found when extracting micrometeorites from sedimentary rocks given their small size, so we do not consider them to better represent collected data. The smallest micrometeorite found by Tomkins *et al.* was $\sim 4 \mu\text{m}$ in radius. Second, we do not consider fully oxidized or unoxidized micrometeorites (i.e., pure FeO or pure Fe). This is done as pure Fe micrometeorites only exist in our model because they enter the atmosphere slow enough, or with a shallow enough angle that they do not reach the Fe melting temperature. These unmelted micrometeorites represent a fixed feature in the model data that cannot inform of atmospheric composition. Pure FeO micrometeorites represent the limit of our model calculations, so aside from showing their production is expected from the model (dashed blue curve in Fig. 3), they are not considered when calculating the mean Fe fractional area (black/orange lines in Figs. 2 and 3). Neglecting these edge cases does not hinder our ability to reproduce modern micrometeorite data (Fig. 4) since we exclude fully oxidized micrometeorites from the collected data as well, ensuring our data sets are comparable.

To validate our model for modern Earth, we simulated 500 micrometeorites entering modern Earth's O_2 -rich atmosphere. We compare the fractional unoxidized metallic Fe area of modeled micrometeorites to that of micrometeorites collected from Antarctica (15). The results of this comparison are shown in Fig. 4, with our simulated micrometeorites shown in blue and the modern micrometeorite data shown in orange. Our model is only defined while metallic Fe remains in the micrometeorites, so we compare only partially oxidized micrometeorites from both the data and our model. The agreement of the model mean and the data mean from (15) (Fig. 4) indicates that our model can predict the Fe fractional area in modern micrometeorites entering Earth's O_2 -rich atmosphere.

Initial micrometeorite distributions

Using the model described above, we randomly generated micrometeorites from initial mass, velocity, and impact angle distributions. These distributions are described in detail in Love and Brownlee (34) and summarized below. For the initial impact angle, values between 0° and 90° are valid. The fraction of particles with impact angle θ between θ_1 and θ_2 is given by $n(\theta_1, \theta_2) = \sin^2\theta_2 - \sin^2\theta_1$. The equivalent probability density function for θ is given by

$$P(\theta) = \sin(2\theta), \quad 0^\circ < \theta < 90^\circ \quad (17)$$

which we use to randomly sample initial impact angles in this work. In our simulations, micrometeorites with initial impact angles greater than $\sim 83^\circ$ could "skip" off the top of the atmosphere. We stopped the simulation on such particles as soon as they began moving away from Earth to avoid long computation times. Only particles that continued into the atmosphere upon contact were calculated. Micrometeorites with initial angles greater than 83° represent less than 1.5% of the distribution, so the impact of neglecting such particles is likely small.

The initial velocity distribution is defined by $\lambda(v, v + dv) = 1.791 \times 10^5 v^{-5.394} dv$ for velocity, v (in km s^{-1}). The probability density function for v is then given by

$$P(v) = 1.791 \times 10^5 v^{-5.394} \quad (18)$$

for $v > 11.2 \text{ km s}^{-1}$. In this work, we only consider initial velocities up to 20 km s^{-1} . Initial velocities between 11.2 and 20 km s^{-1} represent over 92% of the distribution and is similar to the velocity limits used by both MG and LB. Micrometeorites entering the atmosphere faster than 20 km s^{-1} require an increasingly small time step to avoid numerical errors, which is detrimental to the overall runtime of the simulation. As such, we neglect unusual micrometeorites with velocities greater than 20 km s^{-1} and expect it should have little bearing on our final results.

The initial mass distribution of the cumulative number of particles of mass greater than m per square meter per second is defined by

$$F(m) = (2.2 \times 10^3 m^{0.306} + 15)^{-4.38} + 1.3 \times 10^{-9} (m + 10^{11} m^2 + 10^{27} m^4)^{-0.36} \quad (19)$$

This function is defined at 1 AU for particles greater than $\sim 10^{-14} \text{ g}$. We only consider masses between 2.346×10^{-9} and $2.932 \times 10^{-2} \text{ g}$, which correspond to initial Fe particle radii of 2 and $1000 \mu\text{m}$, respectively. The collected micrometeorites we compare to were all greater than $2 \mu\text{m}$ in radius, which is how we set the lower limit. Our model assumes that the micrometeorite radius is less than its mean free path in the upper atmosphere, which is only true for small particles. At $1000\text{-}\mu\text{m}$ radius, this assumption becomes less reasonable, and such large particles could develop a bow shock, which we do not consider. As such, our simulation of the largest particles ($\geq 1000\text{-}\mu\text{m}$ radius) is uncertain. Fortunately, over 95% of the mass distribution results in particles with radii under $500 \mu\text{m}$. Following Love and Brownlee (34), we normalize the above mass distribution between the mass range of interest to find the probability density function

$$P(m) = \frac{(2.2 \times 10^3 m^{0.306} + 15)^{-4.38} + 1.3 \times 10^{-9} (m + 10^{11} m^2 + 10^{27} m^4)^{-0.36}}{4.59811 \times 10^{-13}} \quad (20)$$

for mass m in grams.

Statistical analysis

For our analysis of model uncertainty, we assumed the model output was Gaussian. In addition, we assumed that the two data points available from Tomkins *et al.* formed a Gaussian and used them to calculate a mean and SD. The estimate from the Tomkins *et al.* data should be viewed with skepticism until additional data are collected. The code necessary to reproduce our analysis is included in the Supplementary Materials.

SUPPLEMENTARY MATERIALS

Supplementary material for this article is available at <http://advances.sciencemag.org/cgi/content/full/6/4/eaay4644/DC1>

Data file S1. A zipped file containing our model as a Python script and the data files necessary to reproduce our results and figures.

Movie S1. An animated version of Fig. 1. The movie also shows a simulated micrometeorite (gray sphere) and the corresponding micrometeorite cross section.

REFERENCES AND NOTES

1. J. F. Kasting, Earth's early atmosphere. *Science* **259**, 920–926 (1993).
2. J. Krissansen-Totton, G. N. Arney, D. C. Catling, Constraining the climate and ocean pH of the early Earth with a geological carbon cycle model. *Proc. Natl. Acad. Sci. U.S.A.* **115**, 4105–4110 (2018).

3. D. C. Catling, J. F. Kasting, *Atmospheric Evolution on Inhabited and Lifeless Worlds* (Cambridge Univ. Press, New York, 2017).
4. R. E. Blake, S. J. Chang, A. Lepland, Phosphate oxygen isotopic evidence for a temperate and biologically active Archean ocean. *Nature* **464**, 1029–1032 (2010).
5. M. T. Hren, M. M. Tice, C. P. Chamberlain, Oxygen and hydrogen isotope evidence for a temperate climate 3.42 billion years ago. *Nature* **462**, 205–208 (2009).
6. M. J. de Wit, H. Furnes, 3.5-Ga hydrothermal fields and diamictites in the Barberton Greenstone Belt—Paleoarchean crust in cold environments. *Sci. Adv.* **2**, e1500368 (2016).
7. L. P. Knauth, D. R. Lowe, High Archean climatic temperature inferred from oxygen isotope geochemistry of cherts in the 3.5 Ga Swaziland Supergroup, South Africa. *GSA Bull.* **115**, 566–580 (2003).
8. P. Fralick, J. E. Carter, Neoproterozoic deep marine paleotemperature: Evidence from turbidite successions. *Precambrian Res.* **191**, 78–84 (2011).
9. E. A. Gaucher, S. Govindarajan, O. K. Ganesh, Palaeotemperature trend for Precambrian life inferred from resurrected proteins. *Nature* **451**, 704–707 (2008).
10. A. G. Tomkins, L. Bowl, M. Genge, S. A. Wilson, H. E. A. Brand, J. L. Wykes, Ancient micrometeorites suggestive of an oxygen-rich Archean upper atmosphere. *Nature* **533**, 235–238 (2016).
11. P. B. Rimmer, O. Shorttle, S. Rugheimer, Oxidised micrometeorites as evidence for low atmospheric pressure on the early Earth. *Geochem. Perspect. Lett.* **9**, 38–42 (2019).
12. J. Farquhar, A. L. Zerkle, A. Bekker, Reference module in Earth system and environmental sciences, in *Treatise on Geochemistry*, H. Holland, K. Turekian, Eds. (Elsevier Ltd., ed. 2, 2014), pp. 91–138.
13. K. Zahnle, R. Buick, Atmospheric science: Ancient air caught by shooting stars. *Nature* **533**, 184–186 (2016).
14. M. J. Genge, The origins of I-type spherules and the atmospheric entry of iron micrometeoroids. *Meteorit. Planet. Sci.* **51**, 1063–1081 (2016).
15. M. J. Genge, B. Davies, M. D. Suttle, M. van Ginneken, A. G. Tomkins, The mineralogy and petrology of I-type cosmic spherules: Implications for their sources, origins and identification in sedimentary rocks. *Geochim. Cosmochim. Acta* **218**, 167–200 (2017).
16. C. E. Harman, E. W. Schwieterman, J. C. Schottelkotte, J. F. Kasting, Abiotic O₂ levels on planets around F, G, K, and M stars: Possible false positives for life? *Astrophys. J.* **812**, 137 (2015).
17. A. E. Krull-Davatzes, G. R. Byerly, D. R. Lowe, Evidence for a low-O₂ Archean atmosphere from nickel-rich chrome spinels in 3.24 Ga impact spherules, Barberton greenstone belt, South Africa. *Earth Planet. Sci. Lett.* **296**, 319–328 (2010).
18. J. Farquhar, H. Bao, M. Thiemens, Atmospheric influence of Earth's earliest sulfur cycle. *Science* **289**, 756–759 (2000).
19. A. A. Pavlov, J. F. Kasting, Mass-independent fractionation of sulfur isotopes in Archean sediments: Strong evidence for an anoxic Archean atmosphere. *Astrobiology* **2**, 27–41 (2002).
20. K. Zahnle, M. Claire, D. Catling, The loss of mass-independent fractionation in sulfur due to a Palaeoproterozoic collapse of atmospheric methane. *Geobiology* **4**, 271–283 (2006).
21. M. Sliapski, B. M. Jakosky, M. Benna, M. Elrod, P. Mahaffy, D. Kass, S. Stone, R. Yelle, Variability of martian turbopause altitudes. *J. Geophys. Res. Planets* **123**, 2939–2957 (2018).
22. S. M. Som, R. Buick, J. W. Hagadorn, T. S. Blake, J. M. Perreault, J. P. Harnmeijer, D. C. Catling, Earth's air pressure 2.7 billion years ago constrained to less than half of modern levels. *Nat. Geosci.* **9**, 448–451 (2016).
23. S. M. Som, D. C. Catling, J. P. Harnmeijer, P. M. Polivka, R. Buick, Air density 2.7 billion years ago limited to less than twice modern levels by fossil raindrop imprints. *Nature* **484**, 359–362 (2012).
24. S. T. Massie, D. M. Hunten, Stratospheric eddy diffusion coefficients from tracer data. *J. Geophys. Res.* **86**, 9859–9868 (1981).
25. M. L. Smith, M. W. Claire, D. C. Catling, K. J. Zahnle, The formation of sulfate, nitrate and perchlorate salts in the martian atmosphere. *Icarus* **231**, 51–64 (2014).
26. Y. Kanzaki, T. Murakami, Estimates of atmospheric CO₂ in the Neoproterozoic–Paleoproterozoic from paleosols. *Geochim. Cosmochim. Acta* **159**, 190–219 (2015).
27. H. T. Abuluwefa, R. I. L. Guthrie, F. Ajersch, Oxidation of low carbon steel in multicomponent gases: Part I. Reaction mechanisms during isothermal oxidation. *Metall. Mater. Trans. A* **28**, 1633–1641 (1997).
28. V. N. Smirnov, Rate constant of the gas-phase reaction between Fe atoms and CO₂. *Kinet. Catal.* **49**, 607–609 (2008).
29. T. W. Lyons, C. T. Reinhard, N. J. Planavsky, The rise of oxygen in Earth's early ocean and atmosphere. *Nature* **506**, 307–315 (2014).
30. K. J. Zahnle, M. Gacesa, D. C. Catling, Strange messenger: A new history of hydrogen on Earth, as told by Xenon. *Geochim. Cosmochim. Acta* **244**, 56–85 (2019).
31. E. e. Stüeken, M. A. Kipp, M. C. Koehler, E. W. Schwieterman, B. Johnson, R. Buick, Modeling pN₂ through geological time: Implications for planetary climates and atmospheric biosignatures. *Astrobiology* **16**, 949–963 (2016).
32. G. Arney, S. D. Domagal-Goldman, V. S. Meadows, E. T. Wolf, E. Schwieterman, B. Charnay, M. Claire, E. Hébrard, M. G. Trainer, The pale orange dot: The spectrum and habitability of hazy Archean Earth. *Astrobiology* **16**, 873–899 (2016).
33. S. Tianrui, H. Zhengjun, W. Yusheng, L. Yanxue, A study of mesoproterozoic iron cosmic micro-spherules from 1.8 Ga and 1.6 Ga old strata in the Ming Tombs District, Beijing. *Acta Geol. Sin. Engl. Ed.* **81**, 649–657 (2007).
34. S. G. Love, D. E. Brownlee, Heating and thermal transformation of micrometeoroids entering the Earth's atmosphere. *Icarus* **89**, 26–43 (1991).
35. I. Crossen, J. Sanz-Forcada, F. Favata, O. Witasse, T. Zegers, N. F. Arnold, Habitat of early life: Solar X-ray and UV radiation at Earth's surface 4–3.5 billion years ago. *J. Geophys. Res. Planets* **112**, 10.1029/2006JE002784, (2007).
36. J. D. Cox, D. D. Wagman, V. A. Medvedev, *CODATA Key Values for Thermodynamics* (Hemisphere Publishing Corp, ed. 1, 1984).
37. M. W. Chase, *NIST-JANAF Thermochemical Tables, Fourth Edition* (Journal of Physical and Chemical Reference Data Monographs, ed. 4, 1998).
38. S. Stolen, R. Glöckner, F. Gronvold, T. Atake, S. Izumisawa, Heat capacity and thermodynamic properties of nearly stoichiometric wüstite from 13 to 450 K. *Am. Mineral.* **81**, 973–981 (2015).
39. J. Wang, A. M. Davis, R. N. Clayton, T. K. Mayeda, *Kinetic isotope fractionation during the evaporation of iron oxide from the liquid state* (Lunar and Planetary Institute, 1994), pp. 1459–1460.

Acknowledgments: We thank M. Genge and S. Olson for the helpful, constructive reviews, and K. Zahnle for the insightful comments and guidance on micrometeorite oxidation via CO₂. **Funding:** This work was supported by the NASA Pathways Program, the University of Washington Astrobiology Program, the Virtual Planetary Laboratory at the University of Washington, the Simons Collaboration on the Origin of Life grant 51170 awarded to D.C.C., NASA Exobiology grant NNX15AL23G, and the NASA Astrobiology Program Grant Number 80NSSC18K0829, and benefited from participation in the NASA Nexus for Exoplanet Systems Science research coordination network. **Author contributions:** O.R.L. developed and implemented the model, performed data collection and analysis, and wrote the manuscript. D.C.C. provided insight on the model and data analysis and helped improve the manuscript. R.B. provided guidance on Archean geology. D.E.B. provided insight on the model and current micrometeorite data. S.N. provided support in micrometeorite data collection. **Competing interests:** The authors declare that they have no competing interests. **Data and materials availability:** The code and data used to generate the figures and perform all model calculations are available in the Supplementary Materials (model provided as a Python script). Additional data related to this paper may be requested from the authors.

Submitted 20 June 2019
 Accepted 8 November 2019
 Published 22 January 2020
 10.1126/sciadv.aay4644

Citation: O. R. Lehmer, D. C. Catling, R. Buick, D. E. Brownlee, S. Newport, Atmospheric CO₂ levels from 2.7 billion years ago inferred from micrometeorite oxidation. *Sci. Adv.* **6**, eaay4644 (2020).

Atmospheric CO₂ levels from 2.7 billion years ago inferred from micrometeorite oxidation

O. R. Lehmer, D. C. Catling, R. Buick, D. E. Brownlee and S. Newport

Sci Adv **6** (4), eaay4644.

DOI: 10.1126/sciadv.aay4644

ARTICLE TOOLS

<http://advances.sciencemag.org/content/6/4/eaay4644>

SUPPLEMENTARY MATERIALS

<http://advances.sciencemag.org/content/suppl/2020/01/17/6.4.eaay4644.DC1>

REFERENCES

This article cites 33 articles, 5 of which you can access for free
<http://advances.sciencemag.org/content/6/4/eaay4644#BIBL>

PERMISSIONS

<http://www.sciencemag.org/help/reprints-and-permissions>

Use of this article is subject to the [Terms of Service](#)

Science Advances (ISSN 2375-2548) is published by the American Association for the Advancement of Science, 1200 New York Avenue NW, Washington, DC 20005. The title *Science Advances* is a registered trademark of AAAS.

Copyright © 2020 The Authors, some rights reserved; exclusive licensee American Association for the Advancement of Science. No claim to original U.S. Government Works. Distributed under a Creative Commons Attribution License 4.0 (CC BY).

advances.sciencemag.org/cgi/content/full/6/4/eaay4644/DC1

Supplementary Materials for

Atmospheric CO₂ levels from 2.7 billion years ago inferred from micrometeorite oxidation

O. R. Lehmer*, D. C. Catling, R. Buick, D. E. Brownlee, S. Newport

*Corresponding author. Email: info@lehmer.us

Published 22 January 2020, *Sci. Adv.* **6**, eaay4644 (2020)
DOI: 10.1126/sciadv.aay4644

Other Supplementary Material for this manuscript includes the following:

(available at advances.sciencemag.org/cgi/content/full/6/4/eaay4644/DC1)

Data file S1 (.zip format). A zipped file containing our model as a Python script and the data files necessary to reproduce our results and figures.

Movie S1 (.mp4 format). An animated version of Fig. 1. The movie also shows a simulated micrometeorite (gray sphere) and the corresponding micrometeorite cross section.